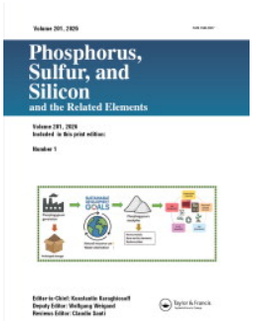

Phosphorus, Sulfur, and Silicon and the Related Elements

ISSN: 1042-6507 (Print) 1563-5325 (Online) Journal homepage: www.tandfonline.com/journals/gpss20

Lipoic acid as a linker to auranofin analogue on nanocellulose

Elisa Bianchi, Francesca Mancusi , Simone La Spina , Lara Massai, Giacomo Biagiotti , Costanza Montis , Luigi Messori , Mirko Severi , Paolo Paoli , Stefano Cicchi & Barbara Richichi

To cite this article: Elisa Bianchi, Francesca Mancusi , Simone La Spina , Lara Massai, Giacomo Biagiotti , Costanza Montis , Luigi Messori , Mirko Severi , Paolo Paoli , Stefano Cicchi & Barbara Richichi (11 Mar 2026): Lipoic acid as a linker to auranofin analogue on nanocellulose, Phosphorus, Sulfur, and Silicon and the Related Elements, DOI: 10.1080/10426507.2026.2640177

To link to this article: https://doi.org/10.1080/10426507.2026.2640177

Published online: 11 Mar 2026.

PHOSPHORUS, SULFUR, AND SILICON AND THE RELATED ELEMENTS
https://doi.org/10.1080/10426507.2026.2640177

Lipoic acid as a linker to auranofin analogue on nanocellulose

Elisa Bianchi[a], Francesca Mancusi[a], Simone La Spina[a], Lara Massai[a], Giacomo Biagiotti[a], Costanza Montis[a,b], Luigi Messori[a], Mirko Severi[a], Paolo Paoli[c], Stefano Cicchi[a], and Barbara Richichi[a]

[a]Department of Chemistry "Ugo Schiff", University of Florence, Sesto Fiorentino (FI), Italy; [b]CSGI, University of Florence, Sesto Fiorentino (FI), Italy; [c]Department of Biomedical, Experimental and Clinical Sciences, Florence, Italy

ABSTRACT

Crystalline nanocellulose (CNC) is a readily available nanostructured form of cellulose, characterized by a high biocompatibility and easily functionalized to produce materials with new properties and applications. In this study, CNC was modified to act as a drug delivery system for the auranofin pharmacophore—specifically, the gold(I)-containing $[Et_3PAu]^+$ moiety. For this purpose, commercial CNC was first derivatized with propargyl groups and subsequently with lipoic acid. These two different functionalizations were then used to insert a simple glucose moiety (as a selector for tumor cells) using a CuAAC reaction with the propargyl end. Meanwhile the lipoic acid S-S bond was reduced with dithiothreitol to react with two equivalents of the gold complex Et_3PAuCl, an analogue of auranofin. The modification of CNC afforded a nanohybrid characterized by a loading of 113.2 mg of Au and 0,41 mmol of selector per g of CNC and by a mean diameter of 290 nm and a Zeta Potential with a value of -51 ± 5 mV. This work opens the possibility of future studies on the use of Auranofin analogues supported on drug delivery systems for biomedical applications. future studies on the use of Auranofin analogues supported on drug delivery systems for biomedical applications.

ARTICLE HISTORY
Received 1 August 2025
Accepted 20 February 2026

KEYWORDS
Nanocellulose; nanomaterials; auranofin; drug delivery

GRAPHICAL ABSTRACT

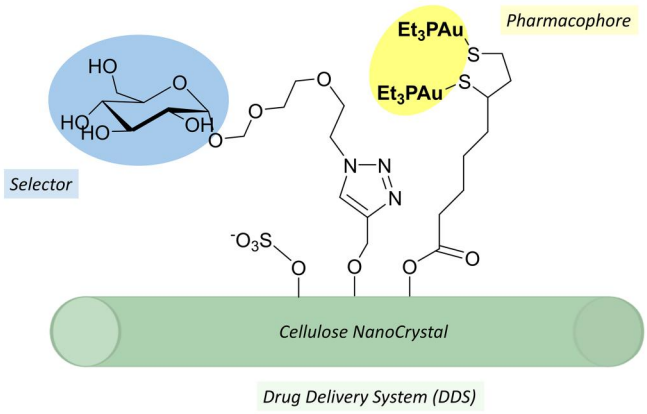

Introduction

Cellulose, the most abundant renewable compound obtained from the biosphere, has been used by our society for thousands of years, and it is still of primary importance as demonstrated by the dimensions of the worldwide industries that transform this material. The knowledge of its hierarchical structure and the request for new nanostructured material have driven the develop of new cellulose micro- and nano-particles that have found new applications related to their high surface area, their high tensile strength, and their biocompatibility.[1] Just to cite nanosized form, three main different form of cellulose nanoparticles have been described: a) nanofibrillar cellulose (NFC), characterized by a high aspect ratio (4–20 nm wide, 500–2000 nm in length) and obtained by mechanical process,[1] but also *via* supercritical CO_2 extraction;[2] b) tunicate cellulose nanocrystals (t-CNC) obtained by acid hydrolysis but also *via* enzymatic treatment of tunicates[3] and finally c) crystalline nanocellulose (CNC).

Crystalline nanocellulose (CNC) is composed by nanorods o whiskers with a diameter ranging from 3 to 50 nm

CONTACT Elisa Bianchi elisa.bianchi1@unifi.it Department of Chemistry "Ugo Schiff", University of Florence, Via della Lastruccia 3–13, 50019, Sesto Fiorentino (FI), Italy.

and length ranging from 50 nm to hundreds of nm,[4,5] and it's characterized by high crystallinity, biocompatibility, biodegradability and high surface area.[5,6] CNC can be conveniently obtained by agricultural[7] or industrial waste material like textile cotton[8] *via* acid or enzymatic treatment.[9] A common procedure is the treatment of cellulose pulp with 64 wt% sulfuric acid.[5] This treatment introduces 0.5–2% of hemisulfate groups providing a net negative charge on each nanocrystal, responsible for the stability of their water dispersions.[5,10] The presence of free hydroxyl groups on the surface of CNC allows a straightforward functionalisation: etherification, esterification, and oxidation with TEMPO (2,2,6,6-Tetramethylpiperidin-1-yl)oxyl) are the most common strategies.[1,6,10] As well, a widely applied strategy for the functionalisation of materials, the CuAAC reaction, has been used to functionalize CNC,[11] opening the door to the potential expansion of the variety of CNC-based materials. The combination of CNC's properties with the easy chemical modifications of nanocellulose to bind and release therapeutic agents,[12] leads to an ideal drug delivery system (DDS) that lately made CNC widely researched for drug delivery systems.[13] Nanocellulose has proved to be a useful carrier for different drug administration routes such as oral, transdermal, and local but, also, its cellular internalization process has been widely studied revealing the different cellular mechanisms involved.[14,15] DDS are suitable to get "old" drugs back in the game, in fact some key points that lead to build a drug delivery system are the efficient uptake of drugs that have solubility issues, a better control of the drug release over a long period of time and reduced drug administration.[16,17] The role of the DDS might also be extended to drugs that are undergoing a repurposing process[18] profiting of their previous clinical studying and offering a more efficient administration route.

Auranofin is an example of a drug that has undergone a repurposing process. It has been used clinically since 1985 to treat rheumatoid arthritis[19], but novel antirheumatic medications are now available.[20] Even though its use as an antirheumatic agent has declined, studies have shown its potential for treating other diseases. Recently, there has therefore been a move to repurpose Auranofin as an antimicrobial and anticancer drug.[20–22] Its activity against breast, ovarian and lung cancer is due to the inhibition of thioredoxin reductase, which is overexpressed in these types of cancer and leads to increased cellular oxidative stress and apoptosis induction.[22] Auranofin structure is characterized by a triethylphosphine Au (I) complex linked to a tetraacetylated thioglucose moiety and studies have shown that the $[Et_3PAu(I)]^+$ moiety is the pharmacophoric unit.[19] It is suggested that upon administration of auranofin, the tetraacetylated thioglucose ligand is rapidly displaced by blood thiols.[23] Then $[Et_3PAu(I)]^+$ species emanating from auranofin reacts to the redox-active selenocysteine or cysteine residues.[24]

On this premise, the grafting of the Auranofin pharmacophore onto a properly substituted CNC provides an opportunity to couple the antitumoral (as well as antimicrobial and anti-parasitic) activity of the Au complex with the delivery efficiency of CNC to produce a new organic-inorganic hybrid characterized by a high loading of Au(I) ions. To this goal, a new DDS was prepared in which CNC was grafted with lipoic acid residues, *via* a simple esterification procedure, and with selecting units represented by a glucoside bearing a short triethylenglycol chain as a spacer. This final functionalisation was grafted using the CuAAC reaction. Previous work has demonstrated the ability of such a selecting unit to increase delivery efficiency toward tumor cells overexpressing Glut-1 receptors.[25,26]

Results and discussion

Scheme 1

The assembling of the DDS started from the reaction of commercial sulfated nanocellulose **1** with propargyl bromide to obtain alkynyl@CNC **2**, a suitable platform for the grafting of the planned glucose-based selector **5** (Scheme 1). Compound **2** was also characterized by Dynamic Light Scattering (DLS) analyses showing a mean hydrodynamic diameter of 577 nm (Figure 2) and a Zeta Potential with a value of −4.2 mV (see Experimental section), suggesting a higher aggregation degree, even after a limited functionalization, if compared with the starting material (82 nm). Following the introduction of alkyne groups, it was the turn of lipoic acid **3**. A simple coupling reaction between the carboxylic end of the acid and the free hydroxyl groups on the CNC allowed the production of compound **4**. The amount of sulfur was evaluated *via* elemental analysis (*see Experimental section*), providing the functionalisation degree with lipoic acid of 0,47 mmol/g. Again, DLS analysis confirmed the nanometric dimensions of the adduct with a mean hydrodynamic diameter of 235 nm (Figure 3) while the negative Z Potential −39 mV guaranteed the stability of its water dispersion (see Experimental section).

Eventually, the selector **5**,[11] glucose and a short pegylated chain, was linked to CNC with a CuAAC reaction between the azide group on the pegylated chain and the alkyne group previously introduced on the substrate, to produce **6**. The quantitative evaluation of the functionalisation degree is a crucial step in the characterization of CNC derivatives.[27] The insertion of the selector was also the occasion to evaluate the original functionalisation degree obtained previously with the insertion of the propargylic group (in

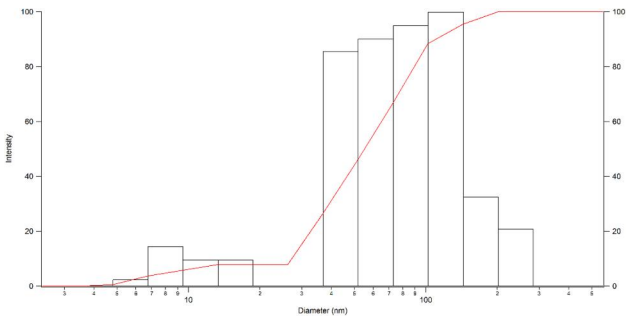

Figure 1. DLS characterization of Compound **1**.

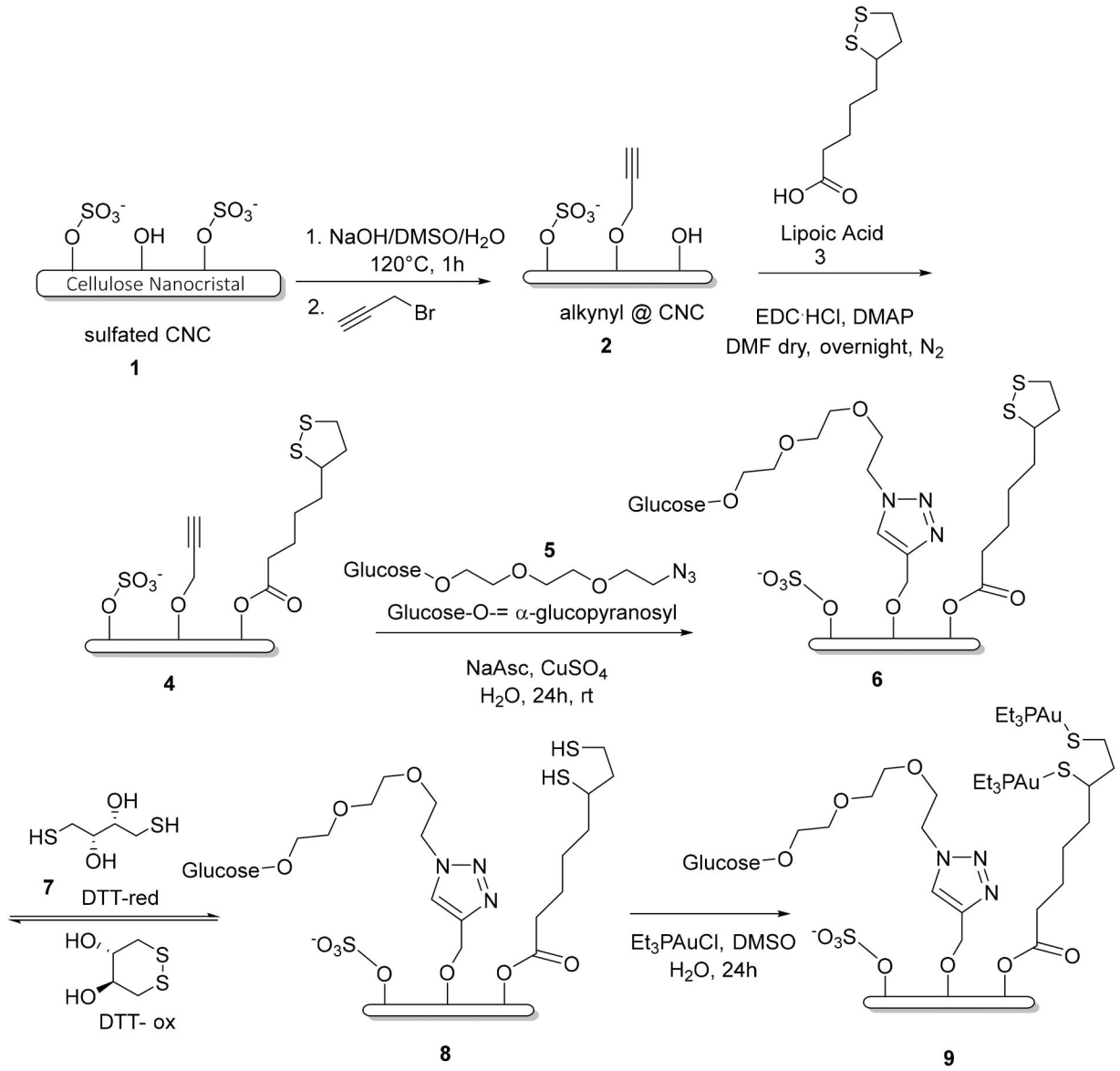

Scheme 1.

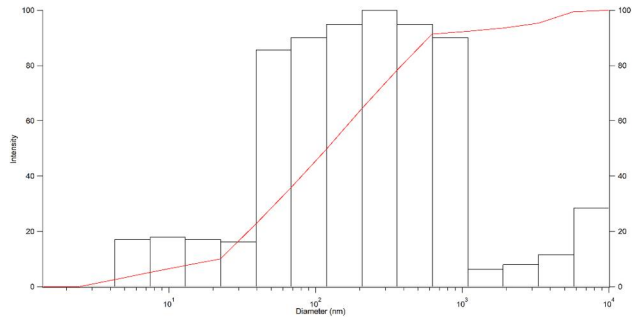

Figure 2. DLS characterization of Compound **2**.

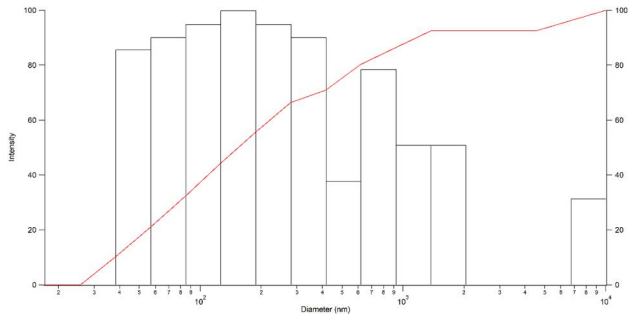

Figure 3. DLS characterization of Compound **4**.

compound **2**). An elemental analysis of the resulting material, after thorough purification *via* centrifugation and extensive dialysis, afforded the value of nitrogen content of the sample and, consequently, the degree of propargylic groups (at least those accessible in the CuAAC reaction) of 0,41 mmol/g. Once again, the compound was characterized by DLS, mean diameter of 190 nm (Figure 4) and a negative Zeta Potential (see Experimental section). With this final decoration, the desired DDS was completed and ready for the loading of the Au(I) complex. This was accomplished profiting of the presence of the lipoic acid after the reduction of the S–S bond.

To reach this goal, 1,3-dithiothreitol (DTT, **7**) was used as a reducing agent. In the presence of DTT, the system reaches

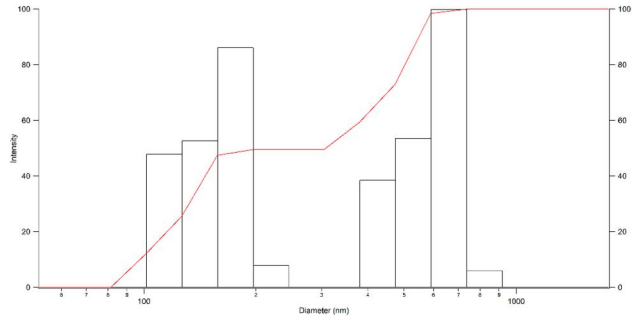

Figure 4. DLS characterization of Compound **6**.

Table 1. ICP analysis of compound **8**.

Reaction time	3 h	6 h	24 h
Au (μg/mg)	83.4 ± 4.17	51.2 ± 2.56	113.2 ± 5.65
μmol Au	0.42	0.26	0.57
μmol S[a]	0.47	0.47	0.47

[a]Calculated from elemental analysis, triplicate.

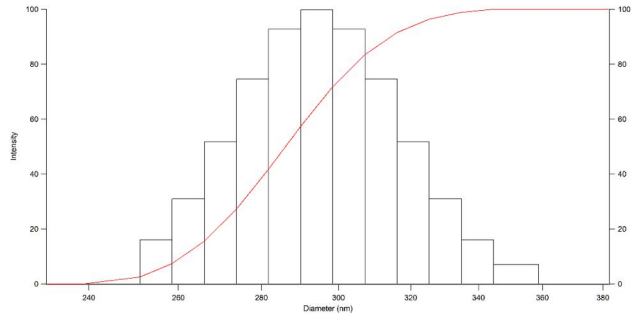

Figure 5. DLS characterization of Compound **9**.

an equilibrium state, so the DTT is added in excess in comparison to the moles of lipoic acid to drive the equilibrium toward the reduced, open-chain form of lipoic acid, as shown in intermediate **8** (Scheme 1).[22] Then Et_3PAuCl is added, leaving the reaction mixture under stirring at room temperature. A simple optimization procedure concerned the reaction time: three identical batches were prepared to afford hybrid **9**. The three batches were left under stirring for 3h, 6h and 24h and the amount of Au was detected *via* ICP analysis (see Table 1). While the batches at 6 and 12 h showed a limited loading, the batch with the higher reaction time shows the highest functionalization with 113.2 μg of Au per mg of CNC. The system was also characterized by DLS that showed a mean diameter of 291 nm (Figure 5) and by Zeta Potential with a value of −51 ± 5 mV.

A critical parameter to monitor during the production of nanosized DDS is represented by the mean hydrodynamic radius of the nanoparticles which can vary greatly depending on the characteristics of the CNC surface decoration. As a matter of fact, the dynamic light scattering analyses (DLS) highlight a net variation moving from commercial **1** (82 nm, producer data, *ζ-potential:* −48 mV) to **2** (mean diameter 577 nm, *ζ-potential:* −4.2 mV). The decoration with a lipophilic substituent as the propargyl group, present in **2**, can be responsible for such behavior. The DLS analysis of **2** (Figure 2, experimental section) show a large dispersion of the hydrodynamic radii, suggesting a certain degree of aggregation. Moving to **4** and **5**, the DLS analyses (Figures 3 and 4, respectively) a decrease of the mean diameter is observed, probably due to the insertion of more polar substituents on CNC, although the systems are still characterized by a larger radius with respect to the raw material. The final DDS **9** shows (Figure 5, experimental section) a nice DLS analysis in which the hydrodynamic radii are collected around a mean value of 291 nm. This can be due to the reduction of the S-S bond of the lipoic acids exposing polar, and acidic, thiol groups which are only partially involved in the interaction with the Au(I) complex.

Experimental section

Materials and methods

Cellulose nanocrystals (CNC) were purchased from CelluForce® (product name CelluForce NCCTM). All the other reagents were purchased from Sigma–Aldrich or TCI and were used without further purification. All the solvents were purchased from Sigma–Aldrich and used directly. Dialysis was performed with Sigma Aldrich cellulose membrane, diameter 33 or 16 cm.

Synthesis of 2

Compound **1** (1 g) was dissolved in DMSO (10 mL) and MilliQ H_2O (10 mL), and then heated under magnetic stirring for 1 h at 120 °C.[28] Once the reaction cooled down to room temperature, NaOH (26 mg, 0.325 mmol) was added, and the reaction was stirred for a further 30 min. After this time Propargyl Bromide (55 µL, 0,65 mmol) was added and left to react for 48h. The mixture was purified with dialysis for 48h in MilliQ H_2O and then lyophilized. Compound **2** (876 mg) was obtained as a white fluffy solid. *ζ-potential*: (−4.2 ± 0.1) mV.

Synthesis of 4

Compound **2** (500 mg) was dissolved in DMF dry (100 mL), followed by DMAP (70 mg, 0.55 mmol) and EDC·HCl (110 mg, 0.72 mmol), and lipoic acid **3** (150 mg, 0.72 mmol). The reaction mixture was let under stirring overnight under N_2. The solution was acidified with a few drops of HCl 0.1 M and then centrifuged at 8000 rpm (3 × 10min), removing the supernatant and washing with EtOH. The collected compound was purified through dialysis for 3 days in MilliQ H_2O. Compound **4** (380 mg) was obtained as a white fluffy solid. Elemental Analysis: *C 44.31%, H 6.57%, S 1.52%. Degree of functionalization: 0,47 mmol/g. ζ-potential: (−39 ± 4) mV.*

Synthesis of 6

Compound **4** (500 mg) was dissolved in H_2O (5 mL) and stirred for 30 min; after that, a solution of Compound **5** (150 mg, 0,44 mmol, excess) in H_2O (5 mL) was added. The dispersion was then added with $CuSO_4$ (0,15 eq vs **5**, 16 mg) and sodium ascorbate (NaAsc 0.5 eq, 10 mg). The reaction mixture was left stirring at room temperature and, after 5 h, a

second addition of the same quantity of the catalyst was added. The mixture was the left under stirring overnight. The dispersion was then purified *via* dialysis in MilliQ H_2O for the first day, then in EDTA 0.1 M to remove Cu excess, and on the third day again in water. Compound **6** (453 mg) was obtained, after lyophilization, as a white fluffy solid. *Elemental Analysis: C 38.14%, H 5.29%, N 1.70%, S 1.50%. Degree of functionalization: 0,41 mmol/g. ζ-potential: (−54 ± 4) mV.*

Synthesis of 9

Compound **6** (50 mg) was degassed under N_2 flow for 1h. Then DTT (5 eq *vs.* lipoic acid functionalization, 18 mg) was dissolved in 0.5 mL of degassed MilliQ H_2O and added to the solution of compound **6**. After stirring the mixture for 30 min, a solution of Et_3PAuCl (4 eq, 33 mg) in DMSO (1 mL) was added and the reaction mixture was left under stirring for 24h. The solution was purified *via* dialysis in MilliQ H_2O for a day. Compound **9**, after freeze-drying (46 mg) was obtained as a grayish fluffy solid. *ICP: Au (113.2 ± 5.65) μg/mg. ζ-potential: (−51 ± 5) mV.*

Inductive coupled plasma atomic emission spectroscopy (ICP-AES)

Before ICP–AES analysis, CNC derivatives have been digested using microwave-assisted mineralization (MARS-Xpress, CEM) with a mixture of suprapure nitric acid obtained by sub-boiling distillation and hydrochloric acid (37%) in a molar ratio 1:3. The determination of Au concentrations was done in triplicate using Ge at a concentration of 1.0 mg/L as internal standard. Wavelengths used for Au determination were 242.794 and 267.594 nm, whereas for Ge, was used the line at 209.426 nm. The ICP operating conditions were optimized to obtain the maximum signal intensity, and between each sample, a rinse solution constituted by 2% v/v of HNO_3 was used.

Dynamic light scattering

DLS measurements at $\theta = 90°$ were performed on 0.1 mg/mL dispersion in H_2O with *90 Plus Particle Size Analyzer, Brookhaven Instruments Corporation.* Obtained autocorrelation functions were analyzed through Contin algorithm, resulting in population distributions of the hydrodynamic diameter of the compounds. In Figures 1–5, DLS data are reported as scattered-intensity weighted size distributions, calculated through Laplace inversion *via* CONTIN algorithm. The mean hydrodynamic diameter of the distribution is calculated as the scattered intensity weighted mean value of the distribution. *ζ-potential* was performed using *90 Plus Particle Size Analyzer, Brookhaven Instruments Corporation.* Reported ζ-potential results are the average of measurements of 5 runs.

Conclusions

The preparation of a complete DDS for the delivery of $[Et_3PAu(I)]^+$ metal fragments was prepared through a combination of esterification and CuAAC reactions. The assembly of a lipoic acid moiety and of a general selector for tumor cells allowed the production of a platform for DDS that was finally loaded with the $[Et_3PAu(I)]^+$ moieties. The reaction with dithiothreitol allowed the reduction of the disulfide group of lipoic acid and the formation of two Au–S bonds. The orthogonal functionalisation procedure allowed the independent decoration of CNC, allowing a significant loading of the Au(I) species (more than 11% w/w) and of the glucose moiety designed as a selector (0.41 mmol/g). The final optimization of the procedure and the biological tests are currently ongoing

Acknowledgements

E.B., S.C., F.M., B.R., G.B., C.M., M.S. thank ("Progetto Dipartimenti di Eccellenza 2023-2027", allocated to the Department of Chemistry "Ugo Schiff").

Author contributions

CRediT: **Elisa Bianchi**: Conceptualization; **Francesca Mancusi**: Investigation; **Simone La Spina**: Investigation; **Lara Massai**: Conceptualization; **Giacomo Biagiotti**: Investigation; **Costanza Montis**: Conceptualization; **Luigi Messori**: Conceptualization; **Mirko Severi**: Investigation; **Paolo Paoli**: Conceptualization; **Stefano Cicchi**: Supervision; **Barbara Richichi**: Supervision.

Disclosure statement

No potential conflict of interest was reported by the author(s).

Funding

No funding was received.

ORCID

Elisa Bianchi http://orcid.org/0009-0009-9708-2033
Lara Massai http://orcid.org/0000-0003-0765-1802

References

[1] Moon, R. J.; Martini, A.; Nairn, J.; Simonsen, J.; Youngblood, J. Cellulose Nanomaterials Review: Structure, Properties and Nanocomposites. *Chem. Soc. Rev.* **2011**, *40*, 3941–3994. DOI: 10.1039/c0cs00108b.

[2] Oyekanmi, A. A.; Khalil, H. P. S. A.; Rahman, A. A.; Mistar, E. M.; Olaiya, N. G.; Alfatah, T.; Bashir, E.; Mariana, M.; Hazwan, C. M.; Abdullah, C. K. Extracted Supercritical CO_2 Cinnamon Oil Functional Properties Enhancement in Cellulose Nanofibre Reinforced Euchema Cottoni Biopolymer Films. *J. Mater. Res. Technol.* **2021**, *15*, 4293–4308. DOI: 10.1016/j.jmrt.2021.10.025.

[3] Lv, X.; Han, J.; Liu, M.; Yu, H.; Liu, K.; Yang, Y.; Sun, Y.; Pan, P.; Liang, Z.; Chang, L.; et al. Overview of Preparation, Modification, and Application of Tunicate-Derived Nanocellulose. *Chem. Eng. J.* **2023**, *452*, 139439. DOI: 10.1016/j.cej.2022.139439.

[4] Thomas, B.; Raj, M. C.; Athira, B. K.; Rubiyah, H. M.; Joy, J.; Moores, A.; Drisko, G. L.; Sanchez, C. Nanocellulose, a Versatile Green Platform: From Biosources to Materials and

Their Applications. *Chem. Rev. Am. Chem. Soc.* **2018**, *118*, 11575–11625. DOI: 10.1021/acs.chemrev.7b00627.

[5] Börjesson, M.; Westman, G. Crystalline Nanocellulose—Preparation, Modification, and Properties. In *Cellulose – Fundamental Aspects and Current Trends*. InTech, **2015**, 159–191. DOI: 10.5772/61899.

[6] Trache, D.; Tarchoun, A. F.; Derradji, M.; Hamidon, T. S.; Masruchin, N.; Brosse, N.; Hussin, M. H. Nanocellulose: From Fundamentals to Advanced Applications. *Front Chem.* **2020**, *8*, 392. Frontiers Media S.A. May 6 DOI: 10.3389/fchem.2020.00392.

[7] Wang, Y.; Wang, Z.; Lin, Y.; Qin, Y.; He, R.; Wang, M.; Sun, Q.; Peng, Y. Nanocellulose from Agro-Industrial Wastes: A Review on Sources, Production, Applications, and Current Challenges. *Food Res. Int.* **2024**, *192*, 114741. DOI: 10.1016/j.foodres.2024.114741.

[8] Rizal, S.; Abdul Khalil, H. P. S.; Oyekanmi, A. A.; Olaiya, N. G.; Abdullah, C. K.; Yahya, E. B.; Alfatah, T.; Sabaruddin, F. A.; Rahman, A. A. Cotton Wastes Functionalized Biomaterials from Micro to Nano: A Cleaner Approach for a Sustainable Environmental Application. *Polymers (Basel)* **2021**, *13*, 1006. DOI: 10.3390/polym13071006.

[9] Olaiya, N. G.; Oyekanmi, A. A.; Hanafiah, M. M.; Olugbade, T. O.; Adeyeri, M. K.; Olaiya, F. G. Enzyme-Assisted Extraction of Nanocellulose from Textile Waste: A Review on Production Technique and Applications. *Bioresour. Technol. Rep.* **2022**, *19*, 101183. DOI: 10.1016/j.biteb.2022.101183.

[10] Habibi, Y. Key Advances in the Chemical Modification of Nanocelluloses. *Chem. Soc. Rev.* **2014**, *43*, 1519–1542. DOI: 10.1039/c3cs60204d.

[11] Biagiotti, G.; Toniolo, G.; Albino, M.; Severi, M.; Andreozzi, P.; Marelli, M.; Kokot, H.; Tria, G.; Guerri, A.; Sangregorio, C.; et al. Simple Engineering of Hybrid Cellulose Nanocrystal-Gold Nanoparticles Results in a Functional Glyconanomaterial with Biomolecular Recognition Properties. *Nanoscale Horiz* **2023**, *8*, 776–782. DOI: 10.1039/d3nh00063j.

[12] Liang, H.; Yin, D.; Shi, L.; Liu, Y.; Hu, X.; Zhu, N.; Guo, K. Surface Modification of Cellulose via Photo-Induced Click Reaction. *Carbohydr. Polym.* **2023**, *301*, 120321. DOI: 10.1016/j.carbpol.2022.120321.

[13] Kupnik, K.; Primožič, M.; Kokol, V.; Leitgeb, M. Nanocellulose in Drug Delivery and Antimicrobially Active Materials. *Polymers (Basel)* **2020**, *12*, 2825. DOI: 10.3390/polym12122825.

[14] Wang, G.; Wang, D.; Bietsch, J.; Chen, A.; Sharma, P. Synthesis of Dendritic Glycoclusters and Their Applications for Supramolecular Gelation and Catalysis. *J. Org. Chem.* **2020**, *85*, 16136–16156. DOI: 10.1021/acs.joc.0c01978.

[15] Behzadi, S.; Serpooshan, V.; Tao, W.; Hamaly, M. A.; Alkawareek, M. Y.; Dreaden, E. C.; Brown, D.; Alkilany, A. M.; Farokhzad, O. C.; Mahmoudi, M. Cellular Uptake of Nanoparticles: Journey Inside the Cell. *Chem. Soc. Rev.* **2017**, *46*, 4218–4244. DOI: 10.1039/c6cs00636a.

[16] Tiwari, G.; Tiwari, R.; Bannerjee, S.; Bhati, L.; Pandey, S.; Pandey, P.; Sriwastawa, B. Drug Delivery Systems: An Updated Review. *Int. J. Pharm. Investig.* **2012**, *2*, 2–11. DOI: 10.4103/2230-973x.96920.

[17] Das, M.; Lalsangi, S.; Santra, S.; Banerjee, R. Nanocellulose as a Carrier for Improved Drug Delivery: Progresses and Innovation. *J. Drug Deliv. Sci. Technol.* **2024**, *97*, 105743. DOI: 10.1016/j.jddst.2024.105743.

[18] Kulkarni, V. S.; Alagarsamy, V.; Solomon, V. R.; Jose, P. A.; Murugesan, S. Drug Repurposing: An Effective Tool in Modern Drug Discovery. *Russ. J. Bioorg. Chem.* **2023**, *49*, 157–166. DOI: 10.1134/S1068162023020139.

[19] Wu, B.; Yang, X.; Yan, M. Synthesis and Structure-Activity Relationship Study of Antimicrobial Auranofin Against ESKAPE Pathogens. *J. Med. Chem.* **2019**, *62*, 7751–7768. DOI: 10.1021/acs.jmedchem.9b00550.

[20] Onodera, T.; Momose, I.; Kawada, M. Potential Anticancer Activity of Auranofin. *Chem. Pharm Bull.* **2019**, *67*, 186–191.

[21] Thangamani, S.; Mohammad, H.; Abushahba, M. F. N.; Sobreira, T. J. P.; Hedrick, V. E.; Paul, L. N.; Seleem, M. N. Antibacterial Activity and Mechanism of Action of Auranofin against Multi-Drug Resistant Bacterial Pathogens. *Sci. Rep.* **2016**, *6*, 22571. DOI: 10.1038/srep22571.

[22] Cassetta, M. I.; Marzo, T.; Fallani, S.; Novelli, A.; Messori, L. Drug Repositioning: Auranofin as a Prospective Antimicrobial Agent for the Treatment of Severe Staphylococcal Infections. *Biometals* **2014**, *27*, 787–791. DOI: 10.1007/s10534-014-9743-6.

[23] Iii, C. F. S. Gold-Based Therapeutic Agents. *Chem. Rev.* **1999**, *I*, 2589–2600.

[24] Angelucci, F.; Sayed, A. A.; Williams, D. L.; Boumis, G.; Brunori, M.; Dimastrogiovanni, D.; Miele, A. E.; Pauly, F.; Bellelli, A. Inhibition of Schistosoma Mansoni Thioredoxin-Glutathione Reductase by Auranofin. Structural and Kinetic Aspects. *J. Biol. Chem.* **2009**, *284*, 28977–28985. DOI: 10.1074/jbc.M109.020701.

[25] Biagiotti, G.; Cazzoli, R.; Andreozzi, P.; Aresta, G.; Francesco, M.; Mangini, C.; di Gianvincenzo, P.; Tobia, C.; Recchia, S.; Polito, L.; et al. Biocompatible Cellulose Nanocrystal-Based Trojan Horse Enables Targeted Delivery of Nano-Au Radiosensitizers to Triple Negative Breast Cancer Cells. *Nanoscale Horiz.* **2024**, *9*, 1211–1218. DOI: 10.1039/d4nh00042k.

[26] Su, L.; Feng, Y.; Wei, K.; Xu, X.; Liu, R.; Chen, G. Carbohydrate-Based Macromolecular Biomaterials. *Chem. Rev. Am. Chem. Soc.* **2021**, *121*, 10950–11029. DOI: 10.1021/acs.chemrev.0c01338.

[27] Foster, E. J.; Moon, R. J.; Agarwal, U. P.; Bortner, M. J.; Bras, J.; Camarero-Espinosa, S.; Chan, K. J.; Clift, M. J. D.; Cranston, E. D.; Eichhorn, S. J.; et al. Current Characterization Methods for Cellulose Nanomaterials. *Chem. Soc. Rev. Chem.*, **2018**, *47*, 2609–2679. DOI: 10.1039/c6cs00895j.

[28] Wang, Y.; Yu, Z.; Dufresne, A.; Ye, Z.; Lin, N.; Zhou, J. Quantitative Analysis of Compatibility and Dispersibility in Nanocellulose-Reinforced Composites: Hansen Solubility and Raman Mapping. *ACS Nano* **2021**, *15*, 20148–20163. DOI: 10.1021/acsnano.1c08100.